Payload/launcher vibration isolation: Mr dampers modeling with fluid compressibility and inertia effects through continuity and momentum equations

Pierrick Jean, Roger Ohayon, Dominique Le Bihan

PAYLOAD/LAUNCHER VIBRATION ISOLATION: MR DAMPERS MODELING WITH FLUID COMPRESSIBILITY AND INERTIA EFFECTS THROUGH CONTINUITY AND MOMENTUM EQUATIONS

PIERRICK JEAN[1,2] , ROGER OHAYON[2] & DOMINIQUE LE BIHAN[1]

(1) Structural Dynamics & Coupled Systems Department - ONERA - 92320 Châtillon – France
(2) Structural Mechanics & Coupled Systems Laboratory - CNAM - 75003 Paris - France
Contact email :pierrick.jean@onera.fr

During launching, a payload is submitted to large vibrations, which may damage it. To get rid of the problem, a solution would be to put an appropriate vibration isolator at the payload/launcher interface. Thus, a soft Isolating Payload Attach Fitting (IPAF) using Magneto-Rheological (MR) dampers is envisaged. In a pre-design phase for the launcher application, a preliminary study of the behaviour of a commercial MR damper (RD-1005-3) and its use in a 1-dof vibration isolator is carried out. In this paper, we report the MR damper behaviour analysis based on fluid and solid mechanics equations. In particular, we investigate chambers fluid compressibility and inertia effects. Then the damper model is used to evaluate the performance of a MR isolator in terms of equivalent transmissibility in passive mode and using skyhook control. The theoretical results will be soon compared to those from an experimental bench in construction.

1 Introduction

During launching, a payload is submitted to large vibrations, which may damage it. A good way to set free from this problem is to isolate the payload from launch vibrations. Different isolation strategies may be considered: passive, active, semi-active and hybrid between the aforementioned strategies. Considering the mechanical constraints of the desired isolation (vibration amplitudes and frequencies), among all those strategies, one is particularly suitable: a soft Payload Attach Fitting (PAF) using MR dampers. In terms of forces and strokes, MR dampers seem to be appropriate thanks to their scalability. Moreover, MR semi-active isolation is said to offer nearly as good performance as active isolation, when using MR dampers with a control loop. Finally, the fail-safe property of MR isolator in passive mode is very attractive for the launcher application.

Before designing a 6-dof MR Isolating PAF (IPAF), MR damper and MR 1-dof isolator behaviours are investigated. In the literature, we can find several modeling approaches. Phenomenological models such as Bouc-Wen and derived models [1], [2] can capture the damper behaviour very well. However, they depend on experimental results to adjust the parameters. Mechanical based models are less predictive but may offer a better comprehension of the damper behaviour, especially hysteresis and force overshoots in the force-velocity plot. In [3], Sims et al. propose a lump parameters model to capture fluid compressibility and inertia effects. In [4], continuity equation taking into account fluid compressibility is used, which exhibit the hysteresis effect. In this paper, a modeling based on fluid and solid dynamics equations is done. The same approach as in [4] is generalised, expressing the momentum equation, which exhibits fluid inertia effects. For this, variable control volumes are particularly convenient. The valve flow is solved numerically using a modified Bingham stress-strain rate law as in [5]. The MR damper behaviour resulting from this model exhibits the hysteretic loop (due to compressibility) and force overshoots (due to chambers fluid inertia) at low piston velocities. The prediction ability of the model will be soon estimated and reported in a

next paper, by comparing model results with those from an experimental bench in construction.

2 Proposed model

In this paper, a theoretical model based on fluid and solid dynamics equations is proposed. It has the advantage of being totally general and independent of experimental identification. The results will be compared to those from an experimental bench using RD-1005-3 damper (Lord Corp.). The diagram of this damper is shown in fig. 1. The damper is well described in [6] and [7]. The damper is single-ended. An accumulator containing N_2 gas (12 cm^3) under pressure (20 bars) is aimed at compensating the fluid displaced by the piston rod (cross-section area A_r) and preventing from fluid cavitation.

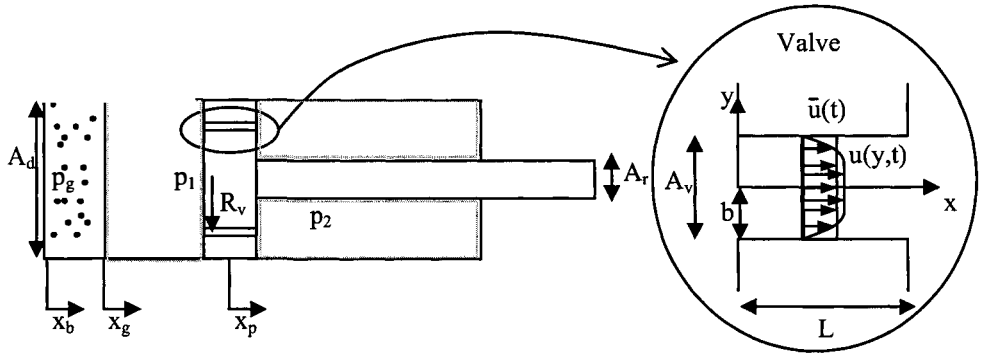

Figure 1. Geometrical parameterization of the MR damper RD-1005-3

2.1 Quasi-steady valve flow model

When flowing from chamber 1 (on the left) to chamber 2 (on the right), the fluid passes through the piston valve. The valve model enables to know the velocity field inside the valve and to relate it to the pressure and drag forces acting on the fluid:

If τ is the shear stress and $\Delta p = p_1 - p_2$, the equation of Navier-Stockes gives:

$$\frac{\Delta p}{L} = \frac{\partial \tau}{\partial y} \quad (1)$$

For want of something better, Lord Corp. data on fluid MRF-132AD [8] are used even if this is not the fluid used in RD-1005-3. The best approach would be to have a set of experimental points from a viscometer on the real fluid. But here we report a method demonstration. Those dates fit well with a modified Bingham law, used in [5]:

$$\tau = \left(\frac{\tau_{yd}(H)}{|\partial u/\partial y| + \varepsilon(H)} + \eta \right) \cdot \frac{\partial u}{\partial y} \quad (2)$$

where η is post-yield viscosity, τ_{yd} the dynamic yield stress and ε a parameter linked to pre-yield viscosity. This law has the advantage of having a continue stress roll-off at small strain rate. Let's call χ the function of equation (2): $\tau = \chi(\partial u/\partial y, H)$.

Thus, to get the velocity profile u(y,H), one has to integrate the stress as follows:

$$u(y,H) = \int_{-b}^{y} \chi^{-1}\left(\frac{\Delta p}{L}\tilde{y}, H\right) d\tilde{y} = \frac{L}{\Delta p} \int_{-\tau_w}^{\tau(y)} \chi^{-1}(\tilde{\tau}, H) d\tilde{\tau} \quad (3)$$

where $\tau_w = \frac{\Delta p}{L} b$ is the wall shear stress and $\tau(y) = \frac{\Delta p}{L} y$, by integrating (1) and taking into account the boundary conditions on the walls (continuity of velocity).

The integration of (3) is numerically done for a range of Δp and H. Then the mean velocity $\overline{u}$ along the cross-section of the valve is calculated. This enables to find two constitutive relations of the valve: $\Delta p = \chi_p(\overline{u}, H)$ (4) and $\tau_w = \chi_\tau(\overline{u}, H)$ (5), which are implemented in the Simulink block diagram (see §4) as look-up tables. Note that the calculus described above is numerical. So it can be applied with any type of stress-strain rate model or set of experimental points.

Finally, the total force of the damper is:

$$F_d = -M_p \ddot{x}_p + p_1(A_d - A_v) - p_2(A_d - A_v - A_r) + 2.\tau_w.2\pi R_v L \quad (6)$$

The last term is introduced in [5]. It represents the viscous drag force. In this simulation, it represents 6.5 % of the pressure force (2nd and 3rd terms).

2.2 Gas accumulator model

If p_{eq} and L_{eq} are the internal gas pressure and equivalent length of the accumulator at the equilibrium piston position, considering that the gas transformation is adiabatic leads to:

$$p_g = \frac{p_{eq}}{(1 + x_g / L_{eq})^\gamma} \cong p_{eq}\left(1 - \gamma \frac{x_g}{L_{eq}}\right) \quad (7)$$

2.3 Chambers model

It is well known that quasi-steady models of the valve are not sufficient to capture the real force-velocity curves of the MR damper, as they exhibit hysteresis and force overshoots at low velocity. To take these dynamic effects into account, [3] build a lump parameters model based on MR fluid compressibility and inertia. [4] build a model based on continuity equation taking into account fluid compressibility. Here, an attempt of generalising this last approach using continuity and momentum equations in variable control volumes of the chambers is done.

In fluid mechanics problems, we can chose fixed or variable control volumes. Here, we chose variable control volumes that follow the chambers volumes. If $V_m(t)$ denotes a material volume and $V_a(t)$ an arbitrary control volume limited by a surface $A_a(t)$, that coincides to $V_m(t)$ at time t, the Reynolds transport theorem gives for a function f :

$$\frac{d}{dt}\int_{V_m(t)} f dV = \frac{d}{dt}\int_{V_a(t)} f dV + \int_{A_a(t)} f(v - w).n dA \quad (8)$$

where v is the fluid velocity, w the velocity of surface $A_a(t)$ and n the surface normal.

Chosen control volumes: $V_{mi}(t)$ a constant quantity of chamber *i* (*i*=1;2) fluid at time t, and $V_{ai}(t)$ the volume delimited by chamber *i* at time t.

Applying $f = \rho$, (fluid density) gives the continuity equation (mass flow rate). So, taking into account the fluid compressibility β as in [4] gives for chambers 1 & 2:

$$\begin{cases} \frac{\dot{m}_1}{\rho} = 0 = A_d(\dot{x}_p - \dot{x}_g) - A_v(\dot{x}_p - \overline{u}) + \frac{V_{a1}}{\beta}\frac{\partial p_1}{\partial t} \\ \frac{\dot{m}_2}{\rho} = 0 = (A_d - A_r)(\dot{x}_b - \dot{x}_p) + A_v(\dot{x}_p - \overline{u}) + \frac{V_{a2}}{\beta}\frac{\partial p_2}{\partial t} \end{cases} \quad (9) \text{ \& } (10)$$

which is of course the same result as in [4] for fixed volume control. The interest of variable control volume is to express momentum equation (applying $f = \rho v$), which expresses the dynamic equation of fluid chambers. The left term in eq. (8) is then equal to the forces sum acting on the fluid. To express the right terms of eq. (8), we have to know the velocity field inside the chamber, which could be done with Computational Fluid Dynamics. Here, we make the following assumption: the velocity field is unidirectional and linearly dependent on the boundaries (piston and gas accumulator frontiers) velocities. Under this assumption, the momentum equation of chamber 1 becomes:

$$\begin{aligned}(p_g - p_1)A_d &= 2\pi R_v \rho \int_{-b}^{b} u^2(y,t)dy - \rho A_v \dot{x}_p \bar{u} \\ &+ \frac{1}{2}\rho\left\{\left(\dot{x}_p - \dot{x}_g\right)\left(A_p\left(\dot{x}_p + \dot{x}_g\right) + A_v\left(\bar{u} + \dot{x}_g\right)\right) + \left(L_1 + x_p - x_g\right)\left(A_p\left(\ddot{x}_p + \ddot{x}_g\right) + A_v\left(\dot{\bar{u}} + \ddot{x}_g\right)\right)\right\}\end{aligned} \tag{11}$$

where $A_p=A_d-A_v$ is the piston surface and L_1 the equilibrium chamber 1 length. This equation enables to bind p_g to p_1, thus making appear the fluid inertia terms acting on the piston. In § 3, we will see how this equation can be simplified by suppressing negligible terms. Note that momentum equation is not written for chamber 2 since it would introduce the pressure on the right side of the damper housing, which is difficult to know.

3 Solving method

The modeling presented in §2 makes appear 5 equations (6), (7), (9), (10), (11) with 5 variables x_g, $\bar{u}$, p_1, p_2, p_g. This system is written in a Simulink block diagram and solved with a simple RK4 integration method. However, due to the complexity of the model, especially equation (11), the system is solved assuming that $p_1=p_g$. After resolution, we can add to the damper force the inertia terms of equation (11). An analysis of the results show that all quadratic velocity terms are very small compared to acceleration terms. Thus the equation (11) can be approximated by:

$$(p_g - p_1)A_d = \frac{1}{2}\rho L_1\left(A_p\left(\ddot{x}_p + \ddot{x}_g\right) + A_v\left(\dot{\bar{u}} + \ddot{x}_g\right)\right) \tag{12}$$

The excitation is a sinusoidal motion of the piston rod, the damper base being fixed. Finally, the damper model is inserted in a 1-dof isolator model consisting of a spring in parallel with the damper, supporting a mass of 50 kg. The isolation frequency of the undamped system is fixed to 5 Hz. The isolator is sinusoidally base-excited. As the isolator is non-linear because of the damper, the output signals are not sinusoidal. However, we can plot the ratio of maximum-output acceleration on maximum-input-acceleration. This transmissibility simulation is solved in the time-domain for a range of input amplitudes and frequencies and plot in the frequency domain.

Both simulations (damper alone and in isolator configuration) will be soon compared with experimental results carried out on an experimental bench in construction using Lord RD-1005-3. The model will be readjusted using experimental results, especially the stress-strain rate curve, which is at present uncertain.

4 Results and discussion

4.1 Hysteresis and MR fluid compressibility

The displacements induced by MR fluid compression are small compared to the piston displacements. However if MR fluid compressibility is neglected, equations (9) and (10) show that $\dot{x}_p$ is proportional to $\bar{u}$, inducing a non-hysteretical law between F_d and $\dot{x}_p$, which is contrary to what is usually observed. As a consequence, fluid compressibility can not be neglected.

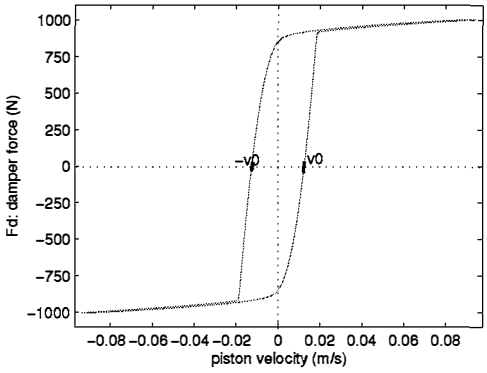

Figure 3. Force-velocity from the model. Sinusoidal motion (5Hz, 3mm)

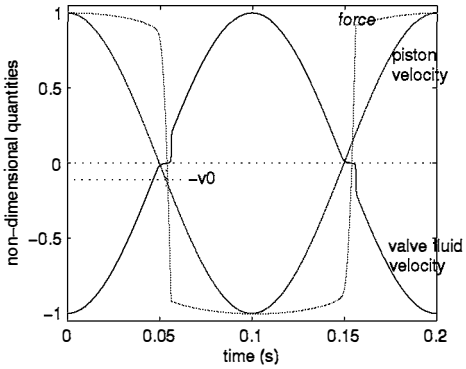

Figure 4. Force, piston velocity, valve velocity Vs time from the model. Same motion as fig. 3

On fig. 3, we can see that the model gives a usual force-velocity curve. Fig.4 enables to understand the hysteresis. The hysteresis is due to a time delay between $\dot{x}_p$ and $\bar{u}$. This delay occurs only at low velocity, when the force changes in sign. The reason of this can be seen from a rearrangement of eqs. (9) and (10), after noting that $\Delta\dot{p} = \frac{\partial \chi_p}{\partial \bar{u}}\dot{\bar{u}} = \chi'_p(\bar{u})\dot{\bar{u}}$ and using eq. (7) to eliminate $\dot{x}_g$:

$$\dot{\bar{u}} + \frac{1}{T(\bar{u})}\bar{u} = -\frac{C}{T(\bar{u})}\dot{x}_p \qquad (13)$$

where C is a multiplicative coefficient due to flow conservation and $T(\bar{u})$ is proportional to $\chi'_p(\bar{u})$. This equation is a first order non-linear differential equation depending on time. However, let's consider for comprehension a biviscous function for $\chi_p(\bar{u})$. Then equation (13) can be split into two domains of $\bar{u}$ (pre-yield and post-yield). For low velocity, $\chi'_p(\bar{u}) = Cpre$, whereas for higher velocity $\chi'_p(\bar{u}) = Cpost$. In our case, $Cpre/Cpost \geq 1400$. As a consequence, the time delay is negligible for high velocities, whereas for low velocities, it is significant. That's exactly what can be observed on fig. 4.

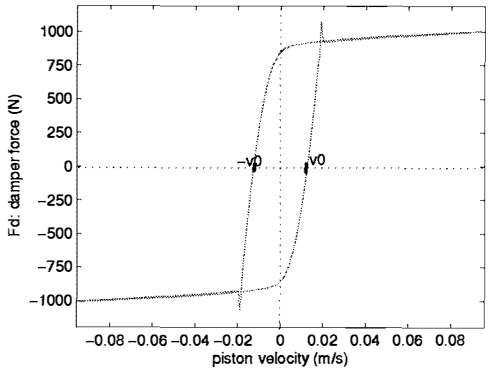

Figure 5. Force-velocity from the model taking fluid inertia into account. Sinusoidal motion (5Hz, 3mm)

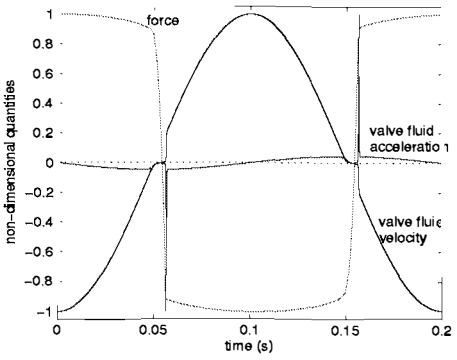

Figure 6. Force, valve velocity and acceleration Vs time from the model. Same motion as fig. 3

4.2 Force overshoots and fluid inertia

Fluid inertia is a possible explanation a commonly observed force overshoots. With the chosen geometry (RD-1005-03), our method gives a negligible fluid inertia force compared to the damper force . The force-velocity curve is similar to fig. 3. However, fluid and gas wall accelerations have a peak (fig.6) when the force is in post-yield region. Fig. 5 is the force-velocity curve from the model taking into account fluid inertia with a quantity of fluid equal to ten times the real quantity. For such an amount of fluid, force overshoots appear. The use of momentum equation seems to be a good way to introduce fluid inertia effect. However, the results should probably be better if the velocity field in the chambers were better known. We will try to enhance this method later.

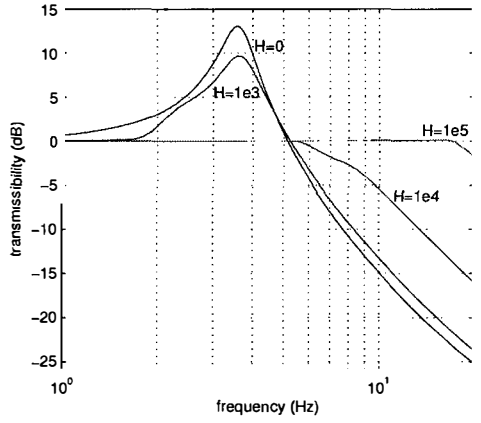

Figure 7. Isolator transmissibility with an amplitude of 1.8mm for different constant magnetic induction (A/m)

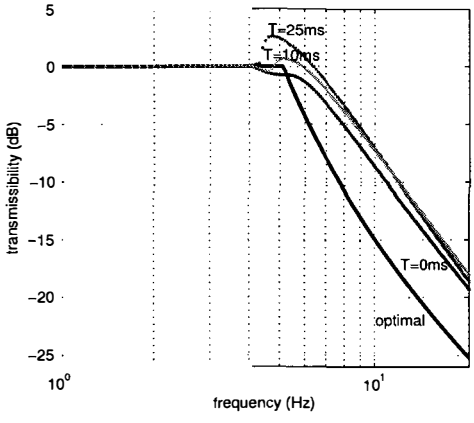

Figure 8. Isolator transmissibility (1.8mm amplitude) : skyhook with different T and optimal

4.3 Single degree of freedom MR isolation

Fig. 7 shows the equivalent transmissibility for different input magnetic inductions. The more H, the less the amplification around resonance, but the worst attenuation above

resonance. Tracking the mimimum transmissibility at each frequency for different H results in an optimal transmissibility curve shown in fig. 8. Using a control law, the transmissibility should tend to this optimal curve as shown in [9]. Fig.8 shows the results for the very known equivalent skyhook control with H_{max}=1e4 A/m.

The magnetic field is created by a current in a coil by following a 1st order transfer function with a time constant T. Fig. 8 shows that the response time damages the isolator performance. Hence the importance to decrease the response time by using either smart coils configuration [10], or PWM (Pulse-Width Modulation) current generation[1]. Note that in this simulation, the transmissibility in the controlled case doesn't tend to the optimal transmissibility. This point will be analyzed and compared with the experiment.

This isolation study is a principle study. The isolation objective in launcher application is -12dB in the [5; 100 Hz] range. Here, for a 1-dof isolator, -12dB is reached in the [13; 100 Hz] range, as shown in fig. 8, nearly without amplificating the input acceleration beneath 13 Hz. In the launcher application, a MR isolator should reach in a similar way the isolation objective from a low frequency F^{MR}_{min} slightly higher than 5 Hz (around 10 to 20 Hz). Then, to complete the isolation frequency range, a hybrid semi-active / active isolator will be investigated, where the active part will have to attenuate in the [5; F^{MR}_{min} Hz] range. Finally, the isolator performance may be enhanced using a three-parameter isolator (added serial spring) as in [10] and by using other control laws.

5 Conclusion

A theoretical analysis of the MR damper behaviour is presented using fluid dynamics equations. As it is a physical approach, it enables a physical comprehension of the damper behaviour (hysteresis and force overshoots). The use of momentum equation seems to be a good manner to introduce fluid inertia effects. However the method has to be enhanced by having a better knowledge of velocity field in the chambers. The theoretical results will be soon compared to experimental results provided by an experimental bench presently in construction. The comparison and enhancement of the modeling will be reported in a next paper. The damper model is then used to predict a single dof MR isolator. The isolation study confirms that MR fluid-based technology seems to be a good way to isolate satellites from launcher vibrations during flight. Some enhancement perspectives of isolator performance are reported: hybrid active/semi-active isolation, three-parameter isolation and optimal control laws will be investigated.

6 Acknowledgments

This paper presents preliminary results of a Doctoral Dissertation carried out by the first author. The authors are thankful to EADS-SPACE Transportation for their partial support. Helpful recommendations of Mr. Sébastien Candel are also appreciated.

References

1. Yang G., Large-scale magnetorheological fluid damper for vibration mitigation: modeling, testing and control. *PhD thesis, University of Notre Dame*, 2001.
2. B.F. Spencer, Jr., S.J. Dyke, M.K. Sain & J.D. Carlson, Phenomenological model of a MR damper, *Journal of Engineering Mechanics, ASCE*, **123** (1997), pp. 230-238

3. Sims N.D., Holmes N.J. & Stanway R., A unified modelling and model updating procedure for electrorheological and magnetorheological vibration dampers. *Smart Materials and Structures*, **13** (2004) pp.100-121.
4. Wang X. & Gordaninejad F., Dynamic modeling of semi-active ER/MR fluid dampers. Damping and Isolation, *Proc. of SPIE Conference on Smart Materials and Structures*, **4331** (2001) pp.82-91.
5. Nishiyama H., Fushimi S. & Nakano M., Numerical simulation of MR fluid damping characteristics using a modified Bingham model. *J. of Intelligent Material Systems and Structures* **13** (2002) pp.647-653.
6. Jolly M.R., Bender J.W. & Carlson J.D., Properties and applications of commercial magnetorheological fluids. *SPIE 5th Annual Int. Symposium on Smart Structures and Materials*. San Diego, CA, March 15, 1998
7. Pang L., Kamath G.M. & Wereley N. M., Analysis and testing of a linear stroke magnetorheological damper. AIAA 98-2040. Vol. CP9803, Part 4, pp.2841-2856
8. http://www.lordcorp.com
9. Choi Y.-T., Wereley N.M. & Jeon Y.-S., Semi-active vibration isolation using magnetorheological isolators. *Damping and Isolation, Proc. of SPIE Conference on Smart Materials and Structures*, **4697** (2002) pp.284-291
10. Kelso S.P. & Henderson B.K., Precision controlled actuation and vibration isolation utilizing magnetorheological fluid technology. AIAA 2001-4568.